eJSSNT Regular Paper

e-Journal of Surface Science and Nanotechnology **17**, 95−100 (2019)

Uncooled Mid-wave Infrared Focal Plane Array Using Band Gap Engineered Mercury Cadmium Telluride Quantum Dot Coated Silicon ROIC

Abhijit Chatterjee,[a,†] Naresh Babu Pendyala,[a] Amardeep Jagtap,[b] K. S. R. Koteswara Rao[b]

[a] *Sensors Development Area, Space Applications Centre (ISRO), Satellite Road, Ahmedabad, 380015, India*
[b] *Department of Physics, Indian Institute of Science, Bangalore, 560012, India*
[†] *Corresponding author: abhijit@sac.isro.gov.in*

Received: 6 June, 2019; Accepted: 1 August, 2019; Published: 8 August, 2019

The dominant photon detectors and focal plane arrays (FPAs) in the mid-wave infrared (MWIR) range (λ = 3 µm to 5 µm) use single crystal InSb and HgCdTe materials. The cost of these detectors is high, and cooling at approximately 80 K to 120 K is required to reduce the dark current. Colloidal quantum dots (CQDs) can be used to provide the speed and detectivity (D^*) of the quantum detectors with lower fabrication costs than those of single crystal epitaxial materials. The aim of this study is to develop a MWIR area array sensor with an HgCdTe-ternary alloyed semiconductor CQD using a commercially available silicon readout integrated circuit (ROIC). First, we synthesized a solution processed HgCdTe CQD responsive in the MWIR range at room temperature and developed a Schottkey junction photodiode array of 10 × 10 pixels based on the same quantum dots (QDs) to produce a HgCdTe-Si interface suitable for a MWIR photodiode at room temperature. After ensuring its functionality, we developed a 320 × 256-pixel focal plane array (FPA) responsive in the MWIR region by hybridization of the HgCdTe CQD layer over a silicon ROIC die with a direct injection input circuit. The FPA was operated using an indigenously developed Field Programmable Gate Array (FPGA)-based drive unit, and different IR targets were imaged to evaluate its use as a low-cost MWIR FPA. NEΔT value of 4 K achieved at room temperature.

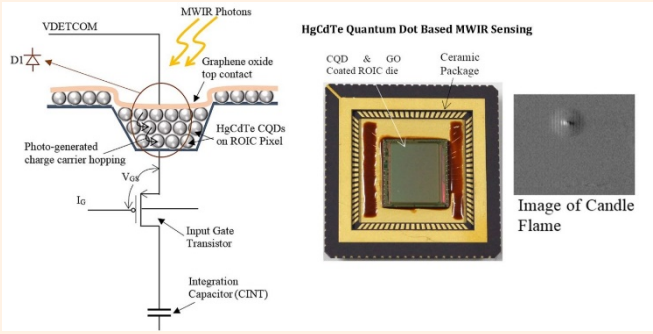

Keywords *FPA; MWIR; HgCdTe; CQD; NEΔT*

I. INTRODUCTION

Remote sensing in the mid-wave infrared (MWIR) spectral range (3−5 µm) is advantageous owing to the atmospheric transmission window. Extensive research has been performed on bulk $Hg_{1-x}Cd_xTe$, for MWIR detection; however, low-temperature cooling is required, which increases the occupied space and energy consumption of the detector, requiring bulky focal plane arrays (FPAs). For quantum dots of a particular composition, the minimum possible band gap is controlled by the composition, and the maximum band gap is based on the size of the particle, which can be tuned using a synthesis method. For quantum dot (QD)-based photodetectors, $Hg_{1-x}Cd_xTe$ is a potential candidate owing to its features, such as a negative band gap E_g = −0.15 eV and large exciton Bohr radius, ensuring the quantum confinement effect at the desired spectral range [1−3]. Significant research work has been carried out for room temperature detection of MWIR radiation and uncooled detector development for this spectral range [4−11] but majority of them involves complex lithographic technique or discrete junction detectors. InAsSb-AlAsSb-nBn detectors are developed [7] and cut-off wavelength achieved close to 4.5 µm at 300 K with D^* value of 5 × 10^9. Discrete responsivity peaks have been observed for hBN/black arsenic phosphorous/hBN detectors [8] in photocon-

ductive mode at λ = 3.4 µm, 5.0 µm, and 7.7 µm. Analytical simulation of PbSe [10] and HgCdTe [11] based detectors have been carried out which also considering pixel structure realizable through complex lithographic technique. We have utilized the advantages of colloidal quantum dots (CQDs) [12−16] with lower fabrication costs [17] to develop MWIR FPA. To develop a MWIR FPA using the advantages of colloidal quantum dots (CQDs), a suitable charge-to-voltage/current conversion circuit is required to extract the photo-generated charge carrier from the QDs and convert it to a measurable quantity, such as the voltage or current. We selected a commercially available 320 × 256-pixel complementary-metal-oxide-semiconductor (CMOS) readout integrated circuit (ROIC) (FLIR ISC9705) [18] for the readout and image generation of the CQDs. The ROIC comprises a direct injection (DI) input cell with a small footprint and low noise and is hybridizable with p- and n-type semiconductors, which are suitable for the development of QD FPAs. Similar ROIC-based FPA developments have been carried out [19−22] however, all are related to shortwave infrared (SWIR) and near infrared (NIR) sensing. MWIR detection has been performed using an HgTe CQD film, and the sample was cooled at 130 K to achieve optimum detectivity.

DI-type ROICs are more suitable for a high-photon flux target. Therefore, we used a high-intensity MWIR source in our test setup. A synthesized HgCdTe CQD was characterized to ensure MWIR absorption and HgCdTe CQD was spin coated over ROIC as a light sensitive layer. Figure 1(a) shows the circuit schematic of a unit cell of the FPA. The detector (D1) is a cluster of QDs that are in physical contact with the readout transistor pad. Figure 1(b) shows a magnified and AFM image of the bare ROIC pixels to determine the pixel depth. Charge carrier transport from one quantum dot (QD) to another follows the hopping phenomenon [23]. Hence, the minority carrier generated through the incident MWIR photon hops through the adjacent QDs and reaches the ROIC source contact of the ROIC pixel DI transistor (Figure 1). The longer ligands of the QD restricts electron movement and increases the resistivity of the CQD film. Therefore, to improve conductivity, the ligand exchange method [24] was used to reduce the ligand length. The column of QDs in contact with the ROIC pixels contribute to the photocurrent. The detector current flows through the input gate transistor and charges the integration capacitor. The anti-blooming gate keeps the input circuit from saturating. The voltage on the integration capacitor is sampled and multiplexed to the column amplifier. The analog output is digitized through a 14-bit analog to digital converter (ADC) and acquired through a NI PXI-based data acquisition system for image formation and data analysis. A 10 × 10-pixel proto device was developed.

Prior to the fabrication of FPA by fabricating $Hg_{1-x}Cd_xTe$/Si heterojunctions with Au and Al contacts for HgCdTe and Si, respectively. A 5 mm × 5 mm-p-type ⟨100⟩ Si wafer piece was used as the substrate. HgCdTe CQD was spin coated over it [after Radio Corporation of America (RCA) cleaning in a wet bench] at 4000 rpm to achieve a uniform thickness of the CQD. A suitable lithography mask was prepared, and 500-µm diameter circular gold contacts were produced using thermal evaporation.

II. FPA DEVELOPMENT AND EXPERIMENTAL

To synthesize CQD, 36 mg of $HgCl_2$ and 4 mg of $CdCl_2$ were added in 4 mL of oleylamine taken in three-necked

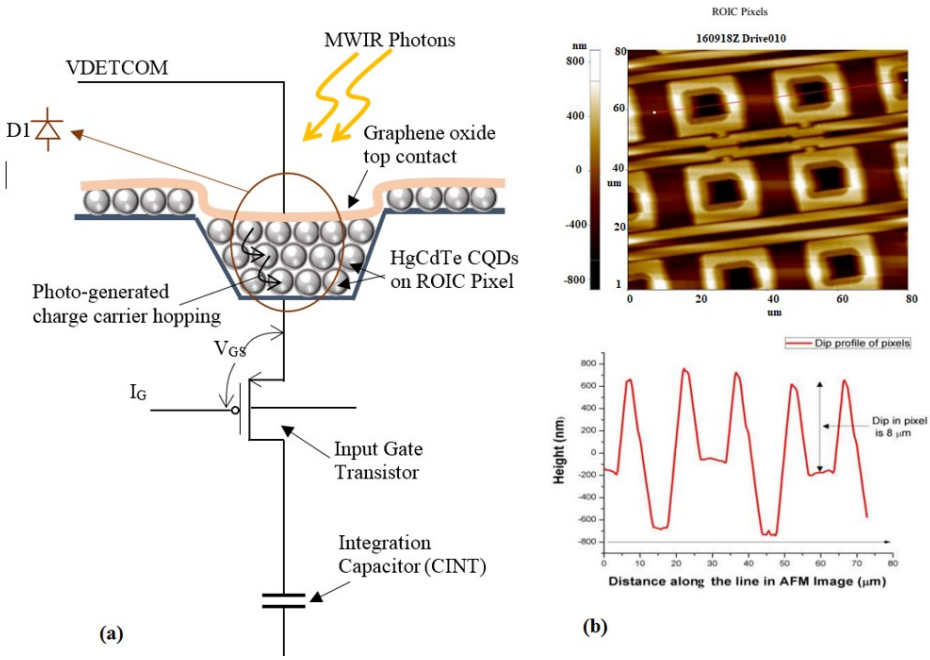

Figure 1: (a) Equivalent circuit schematic of a single pixel of MWIR FPA. (b) AFM of ROIC before CQD coating.

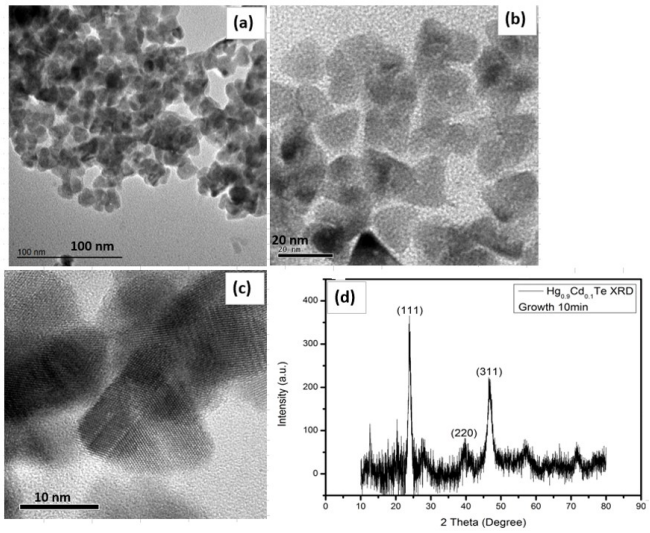

Figure 2: (a) TEM and (b and c) HRTEM images of HgCdTe CQDs with tetrahedral nano-crystal planes (size ≈ 15 nm). (d) XRD plot. Peaks correspond to the (111), (200), (220), (311), (400), and (422) planes of the cubic zinc blende structure of CdTe and HgTe.

flask at 100°C. The molar ratio of Cd/Hg was kept ~0.11. The above mixture was constantly stirred and kept under nitrogen (N_2) ambience by bubbling high purity N_2 gas for an hour at 100°C. After an hour, 0.1 mL from 0.5 M solution of tellurium (Te) precursor in tri-n-octylphosphine (TOP) was injected into the above mixture. A rapidly changing colorless solution from brown to black was noticed, indicating the start of nucleation process and further growth of the particles. Here, the size of the particles could be decided by the growth parameters such as temperature, concentration and the time of growth. In the present study, the aliquots of samples were taken at the interval of 10 min. The photodetector contained an Al/p-Si/HgCdTe CQD/Au geometry. The silicon substrate provided a transmission window for mid-IR radiation (1−10μm) as well as developed a heterojunction [25−28] with the CQDs to facilitate extraction of the photogenerated carrier under a reverse bias condition. Figure 2 shows the TEM images and XRD data of 10 min synthesized HgCdTe CQDs. Interestingly, most of CQDs are in tetrahedral shape [Figure 2(a−c)]. Similar

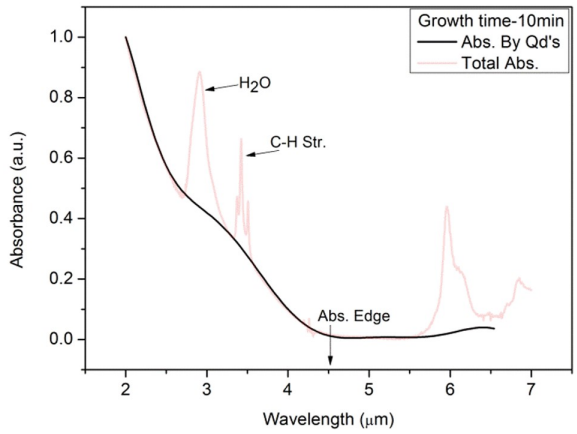

Figure 3: Spectral absorption curve of synthesized HgCdTe CQD through FTIR.

observation of tetrahedral shape was found in the case of HgTe CQDs. This suggests that growth rates for this material are different for different facets. The measured size of 10 min synthesized CQDs is ~10 nm, which is determined from the distance between apex to the opposite side base. X-ray diffraction data [Figure 2(d)] shows three peaks, which corresponds to the (111), (200), (220), (311), (400), and (422) planes of the cubic zinc blende structure of CdTe and HgTe.

For analyzing the excitonic and band edge absorption features, the absorption spectrum is shown in Figure 3. A calibrated black body showed the emission spectrum in the MWIR region as the temperature varied from 300 K to 600 K.

The optical power output of the black body at different temperatures was measured using a DLaTG pyroelectric detector. Furthermore, a high-pass IR filter (Newport Corporation) was mounted in front of the device to ensure that the photon irradiance with a wavelength less than 2.3 μm was eliminated (Figure 4). The device was operated in the photovoltaic mode. An *I*−*V* characterization (Figure 5) of this proto device demonstrated MWIR-sensitive pixel formation, which was replicated in the ROIC-based FPA development. The *I*−*V* characteristics clearly showed photodiode characteristics, and these results are promising for the development of a solution-processed, low-cost, HgCdTe CQD-based FPA.

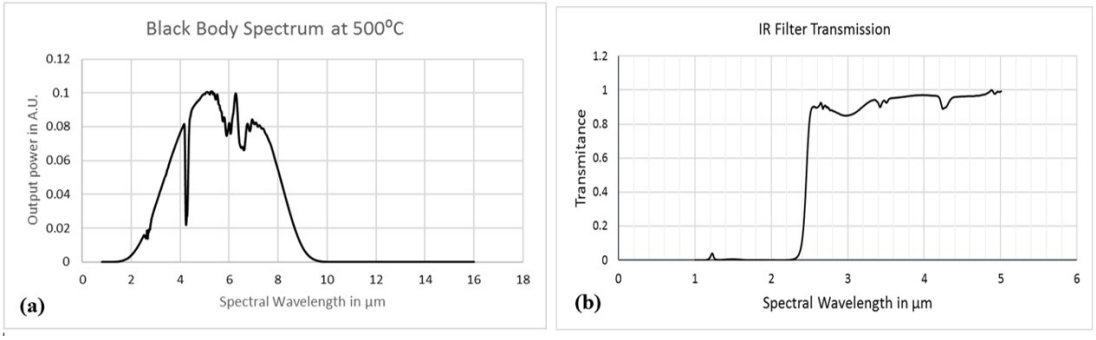

Figure 4: (a) Black body power output. (b) IR high pass filter transmission spectrum.

Initially the ROIC die from the manufacturer that provided a wafer map was cleaned with acetone and isopropyl alcohol (IPA) to remove the photoresist protective layer. Then, the ROIC die was attached to an 84-pin LCC bare package using vacuum compatible epoxy, and wire bonded pads were required to create electrical contacts. A synthesized CQD layer was spin coated over the ROIC surface. After the CQD layer dried, a graphene oxide (GO) layer was dispersed over it to form a top contact that was transparent to MWIR. In previous studies, we showed that GO is an excellent system for electron extraction from photoexcited, NIR-emitting $Hg_{0.2}Cd_{0.8}Te$ CQDs [29]. Implementation of a top contact using ITO resulted in poor transparency in MWIR spectral range. Hence, an ROIC field effect transistor (FET) source contact (VDETCOM) was connected to the GO layer to provide contact with the cathode. The output of the ROIC is an analog voltage, and therefore, a 14-bit, low-noise external ADC was used in the test setup to digitize the sensor data. The FPA is shown in Figure 6. SEM image of QD coating (Figure 7) obtained shows no major pinholes.

A microsemi-FPGA-based circuit was designed and developed to generate the required clocks for the ROIC and ADC. Low dropout voltage regulators (LDO) from Analog Devices were used to generate DC biases for the integrated sensor. Two different printed circuit board (PCBs) were developed. One consisted of FPGA, ADC, and LDO, and the other consisted of a CQD-coated ROIC sensor with decoupling capacitors. A National Instruments data acquisition card (NI6542) was used to acquire the digitized

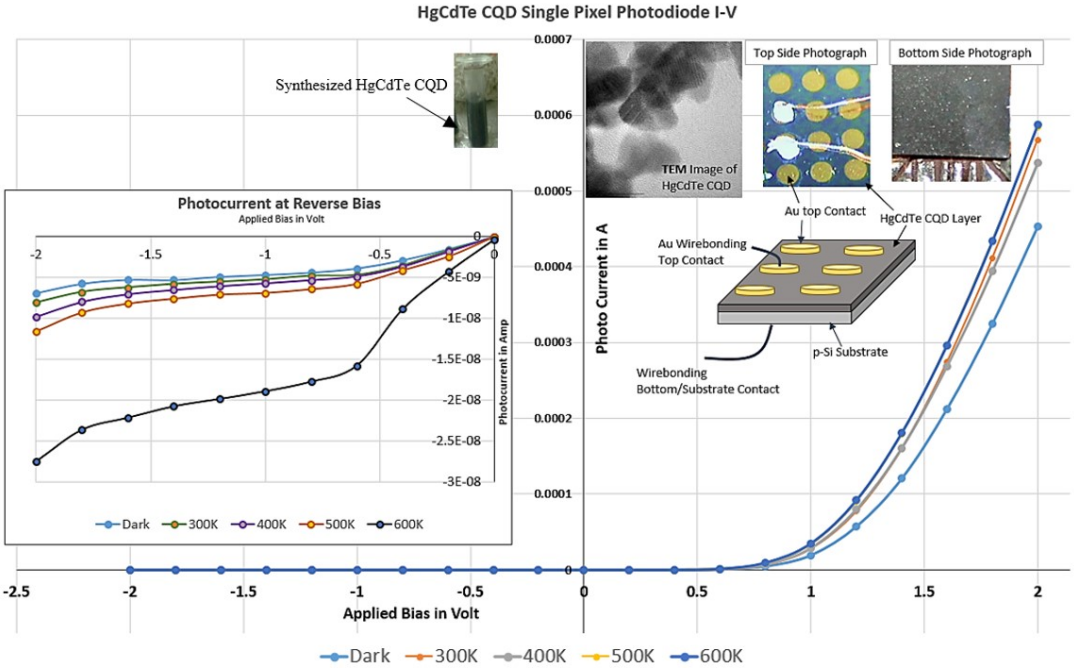

Figure 5: *I–V* characteristics of single junction at different black body temperatures. Proto device photographs, TEM image of HgCdTe quantum dots, and expanded third quadrant plot are in inset. Third quadrant pot depicts photocurrent at different black body temperatures.

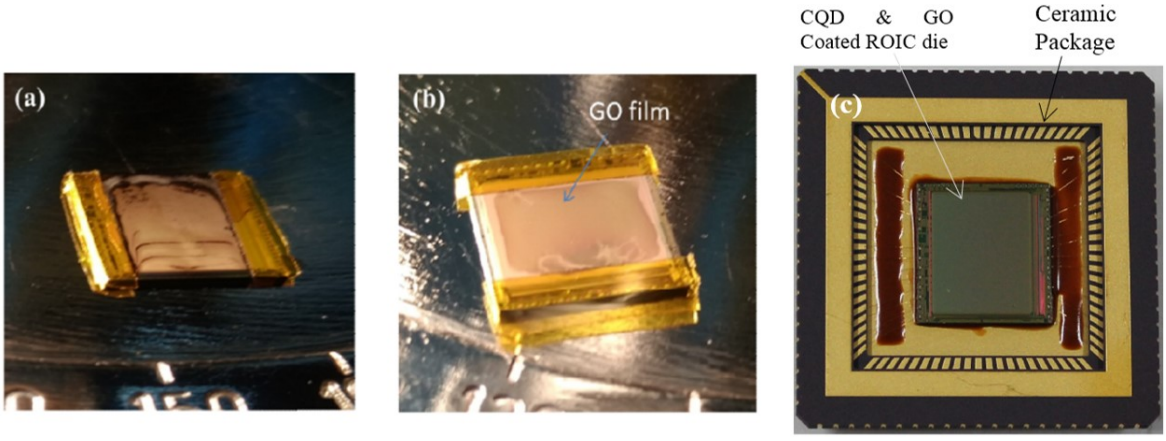

Figure 6: (a) ROIC die coated with HgCdTe CQD. (b) Graphene oxide coated ROIC. (c) FPA realized by wire bonded die on the 84-pin LCC ceramic package.

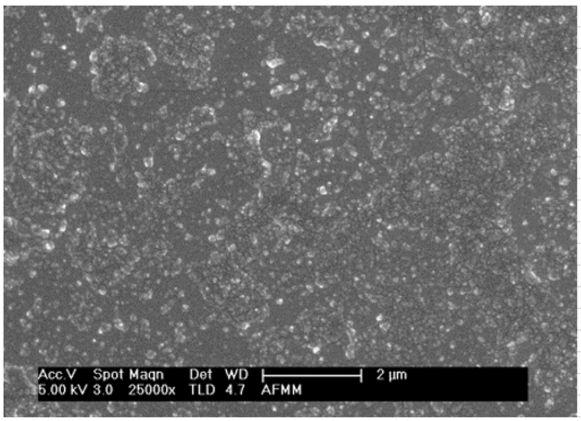

Figure 7: SEM image of HgCdTe QD coating.

sensor data. A block schematic of the MWIR imaging chain is shown in Figure 8. We have computed NEΔT by setting back body at two different temperatures (300 K and 320 K) and 64 frames have been acquired at each temperature. Mean and standard deviation of frame data have been computed for each temperature. Standard deviation over multiple acquisition at dark condition corresponds to dark noise of FPA. NEΔT value comes out to be around 4 K. The human hand and a candle flame were imaged using an IR laser and a ZnSe focusing lens of *f*/4. The images were constructed in LabView GUI software.

III. CONCLUSIONS

An HgCdTe CQD-based MWIR FPA was developed, and imaging at room temperature was performed after confirming the MWIR response from the proto device. We designed and developed an FPGA-based test setup to characterize and perform imaging using ROIC-based imaging sensors. The performance of the setup was validated by imaging different temperature targets. The generated images of the targets with a temperature less than 350 K (e.g., the human body) showed a low SNR at room temperature. This low SNR may be due to non-uniformity of the GO layer and partial absorption of MWIR in this layer [30]. The responsivity can be enhanced by utilizing a core-shell QD structure and a gold nanoparticle-based MWIR transparent top contact [31] over the HgCdTe CQD. Finally, hermetical sealing of the FPAs will be carried out for further screening and qualification to make them suitable for space use.

Acknowledgments

Authors wish to thank S. S. Sarkar (Deputy Director, SEDA), Nilesh Desai (Associate Director, SAC, ISRO), and D. K. Das (Director, SAC, ISRO) for providing the necessary opportunity, facilities and electronic components for carrying out these experiments. Authors also thank Chairman, Department of Physics, Indian Institute of Science, Bangalore and all research scholars of Semiconductor Lab, Department of Physics, IISc for enormous support and motivation.

References

[1] A. Rogalski, Infrared Phys. Technol. **43**, 187 (2002).
[2] A. Rogalski, J. Antoszewski, and L. Faraone, J. Appl. Phys. **105**, 091101 (2009).
[3] W. Lei, J. Antoszewski, and L. Faraone, Appl. Phys. Rev. **2**, 041303 (2015).
[4] V. Daumer, V. Gramich, R. Müller, J. Schmidt, F. Rutz, T. Stadelmann, A. Wörl, and R. Rehm, Proc. SPIE **10177**, 1017711 (2017).
[5] M. A. Kinch, J. Electron. Mater. **47**, 5879 (2018).
[6] M. Kopytko, A. Kębłowski, W. Gawron, P. Madejczyk, A. Kowalewsski, and K. Jóźwikowski, Opto-Electron. Rev. **21**, 402 (2013).
[7] A. Soibel, C. J. Hill, S. A. Keo, L. Hoglund, R. Rosenberg, R. Kowalczyk, A. Khoshakhlagh, A. Fisher, D. Z.-Y. Ting, and S. D. Gunapala, Appl. Phys. Lett. **105**, 023512 (2014).

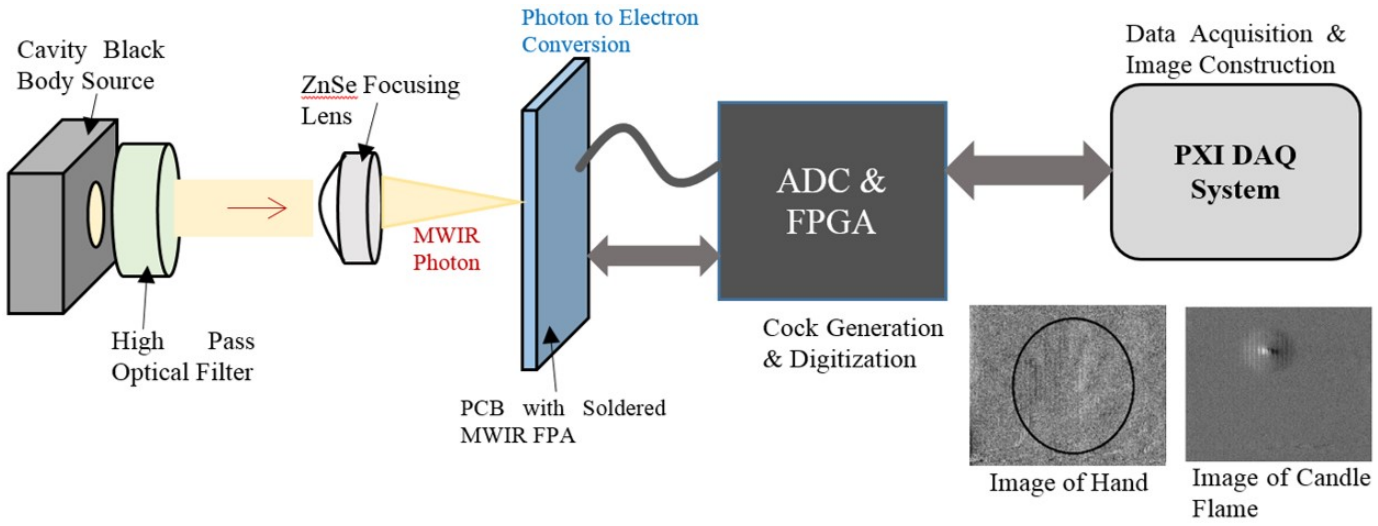

Figure 8: MWIR imaging chain and sample images taken by FPA at room temperature.

[8] S. Yuan, C. Shen, B. Deng, X. Chen, Q. Guo, Y. Ma, A. Abbas, B. Liu, R. Haiges, C. Ott, T. Nilges, K. Watanabe, T. Taniguchi, O. Sinai, D. Naveh, C. Zhou, and F. Xia, Nano Lett. **18**, 3172 (2018).
[9] D. Ren, K. M. Azizur-Rahman, Z. Rong, B.-C. Juang, S. Somasundaram, M. Shahili, A. C. Farrell, B. S. Williams, and D. L. Huffaker, Nano Lett. **19**, 2793 (2019).
[10] R. P. Shea, A. S. Gawarikar, and J. J. Talghader, Opt. Express **18**, 22833 (2010).
[11] V. Srivastav and V. Venkataraman, J. Appl. Phys. **108**, 073112 (2010).
[12] X. Tang, M. M. Ackerman, and P. Guyot-Sionnest, ACS Nano **12**, 7362 (2018).
[13] E. Lhuillier, S. Keuleyan, H. Liu, and P. Guyot-Sionnest, Chem. Mater. **25**, 1272 (2013).
[14] E. Lhuillier, S. Keuleyan, P. Rekemeyer, and P. Guyot-Sionnest, J. Appl. Phys. **110**, 033110 (2011).
[15] M. M. Ackerman, X. Tang, and P. Guyot-Sionnest, ACS Nano **12**, 7264 (2018).
[16] N. Ilyas, D. Li, Y. Song, H. Zhong, Y. Jiang, and W. Li, Sensors **18**, 4163 (2018).
[17] A. J. Ciani, R. E. Pimpinella, C. H. Grein, and P. Guyot-Sionnest, Proc. SPIE **9819**, 981919 (2016).
[18] ISC9705 Standard 320 Specifications, 400-9705-09 Version 1.3, FLIR Systems Inc.
[19] J. B. Barton, R. F. Cannata, and S. M. Petronio, Proc. SPIE **4721**, 37 (2002).
[20] T. R. Hoelter, S. M. Petronio, R. J. Carralejo, J. D. Frank, and J. H. Graff, Proc. SPIE **3698**, 837 (1999).
[21] J. Bundas, K. Patnaude, R. Dennis, D. Burrows, R. Cook, A. Reisinger, M. Sundaram, R. Benson, J. Woolaway, J. Schlesselmann, and S. Petronio, Proc. SPIE **6206**, 62060G (2006).
[22] E. Heves, C. Ozturk, V. Ozguz, and Y. Gurbuz, IEEE Electron Device Lett. **34**, 662 (2013).
[23] R. H. Gilmore, E. M. Y. Lee, M. C. Weidman, A. P. Willard, and W. A.Tisdale, Nano Lett. **17**, 893 (2017).
[24] B. Martinez, C. Livache, N. Goubet, A. Jagtap, H. Cruguel, A. Ouerghi, E. Lacaze, M. G. Silly, and E. Lhuillier, J. Phys. Chem. C **122**, 859 (2018).
[25] J. F. Johnson, IEEE Trans. Electron Devices **46**, 96 (1999).
[26] G. E. Fernandes, J. H. Kim, D. Oller, and J. Xu, Appl. Phys. Lett. **107**, 111111 (2015).
[27] A. Chatterjee and K. S. R. K. Rao, 2018 3rd International Conference on Microwave and Photonics (Dhanbad, India, 2018).
[28] G. Roelkens, U. Dave, A. Gassenq, N. Hattasan, C. Hu, B. Kuyken, F. Leo, A. Malik, M. Muneeb, E. Ryckeboer, S. Uvin, Z. Hens, R. G. Baets, Y. Shimura, F. Gencarelli, B. Vincent, R. Loo, J. V. Campenhout, L. Cerutti, J.-B. Rodriguez, E. Tournié, X. Chen, M. Nedeljkovic, G. Z. Mashanovich, L. Shen, N. Healy, A. C. Peacock, X. Liu, R. M. Osgood, and W. Green, Proc. SPIE **8993**, 899316 (2014).
[29] A. M. Jagtap, V. Varade, B. Konkena, K. P. Ramesh, A. Chatterjee, A. Banerjee, N. B. Pendyala, and K. S. R. K. Rao, J. Appl. Phys. **119**, 074306 (2016).
[30] F. A. Chowdhury, M. A. Hossain, K. Uchida, T. Tamura, K. Sugawa, T. Mochida, J. Otsuki, T. Mohiuddin, M. A. Boby, and M. S. Alam, AIP Adv. **5**, 107228 (2015).
[31] G. Dayal and S. A. Ramakrishna, Opt. Express **20**, 17503 (2012).